Oxygen minimum zone-type biogeochemical cycling in the Cenomanian-Turonian Proto-North Atlantic across Oceanic Anoxic Event 2

Florian Scholz[1]*, Sebastian Beil[2], Sascha Flögel[1], Moritz F. Lehmann[3], Ann Holbourn[2], Klaus Wallmann[1], Wolfgang Kuhnt[2]

[1]GEOMAR Helmholtz Centre for Ocean Research Kiel, Wischhofstraße 1-3, 24111 Kiel, Germany

[2]Marine Micropaleontology, Institute of Geoscience, University of Kiel, Ludewig-Meyn-Straße 14, 24118 Kiel, Germany

[3]Biogeochemistry, Department of Environmental Sciences, University of Basel, Bernoullistrasse 30, 4056 Basel, Switzerland

*Corresponding author. E-mail: fscholz@geomar.de, Phone: +49 (0)431 6002113

Abstract

Oceanic Anoxic Events (OAEs) in Earth's history are regarded as analogues for current and future ocean deoxygenation, potentially providing information on its pacing and internal dynamics. In order to predict the Earth system's response to changes in greenhouse gas concentrations and radiative forcing, a sound understanding of how biogeochemical cycling differs in modern and ancient marine environments is required. Here, we report proxy records for iron (Fe), sulfur and nitrogen cycling in the Tarfaya upwelling system in the Cretaceous Proto-North Atlantic before, during and after OAE2 (~93 Ma). We apply a novel quantitative approach to sedimentary Fe speciation, which takes into account the influence of terrigenous weathering and sedimentation as well as authigenic Fe (non-terrigenous, precipitated onsite) rain rates on Fe-based paleo-redox proxies. Generally elevated ratios of reactive Fe (i.e., bound to oxide, carbonate and sulfide minerals) to total Fe (Fe_{HR}/Fe_T) throughout the 5 million year record are attributed to transport-limited chemical weathering under

greenhouse climate conditions. Trace metal and nitrogen isotope systematics indicate a step-wise transition from oxic to nitrogenous to euxinic conditions over several million years prior to OAE2. Taking into consideration the low terrigenous sedimentation rates in the Tarfaya Basin, we demonstrate that highly elevated Fe_{HR}/Fe_T from the mid-Cenomanian through OAE2 were generated with a relatively small flux of additional authigenic Fe. Evaluation of mass accumulation rates of reactive Fe in conjunction with the extent of pyritization of reactive Fe reveals that authigenic Fe and sulfide precipitation rates in the Tarfaya Basin were similar to those in modern upwelling systems. Because of a smaller seawater nitrate inventory, however, chemolithoautotrophic sulfide oxidation with nitrate was less efficient in preventing hydrogen sulfide release into the water column. As terrigenous weathering and sediment flux determine how much authigenic Fe is required to generate an anoxic euxinic or ferruginous proxy signature, we emphasize that both have to be taken into account when interpreting Fe-based paleo-redox proxies.

Keywords: Oceanic Anoxic Event, iron speciation, nitrogenous, ferruginous, euxinic.

1. Introduction

The world's ocean has experienced multiple episodes of widespread deoxygenation in Earth's history (Jenkyns, 2010; Meyer and Kump, 2012). Most of these Oceanic Anoxic Events (OAEs) were accompanied by biotic crises, some of which are classified as mass extinctions (e.g., the Permian-Triassic Boundary event) (Knoll et al., 1996). In general, OAEs were associated with the emplacement of large igneous provinces, large-scale volcanic carbon dioxide release to the atmosphere and global warming (Arthur et al., 1985). Enhanced chemical weathering under these conditions likely enhanced the terrestrial nutrient supply to the ocean, which in turn amplified primary production and respiratory oxygen (or oxidant) consumption (Monteiro et al., 2012). This trend was exacerbated by reduced oxygen uptake from the atmosphere, related to a diminished solubility of oxygen in warmer seawater, as well as reduced ventilation in a warming ocean (Arthur and Sageman, 1994).

A similar chain of causes and consequences can explain the currently observed trend of ocean deoxygenation. Anthropogenic CO_2 emissions and global warming, together with a globally modified land surface and associated changes in land-ocean fluxes create conditions that are quite similar to major environmental perturbations in Earth history (Diaz and Rosenberg, 2008; Keeling et al., 2010). However, the forcing exerted by volcanic CO_2 is not sufficient to explain the duration of Cretaceous OAEs and the timing of subsequent recovery. Instead, sedimentary recycling of phosphorus (P) and iron (Fe) (Mort et al., 2008; Flögel et al., 2011; Scholz et al., 2018), increased planktonic carbon to P ratios (Flögel et al., 2011), globally increased silicate weathering (Pogge von Strandmann et al., 2013) as well as burial of organic carbon (Arthur et al., 1988; Kuypers et al., 1999; Wallmann et al., 2001) and bio-essential trace metals (Owens et al., 2016) at the seafloor are invoked to explain the temporal and spatial extent of ocean anoxia during these events. Germane to the mismatch between physical forcing and Earth system response in the Cretaceous, only about 50 % of the oxygen decline in the ocean since 1950 can be simulated by state-of-the-art Earth System Models whereas the remaining trend is assigned to feedback mechanisms within marine biogeochemical cycles (Schmidtko et al., 2017; Oschlies et al., 2018).

In order to predict the Earth system's response to changes in greenhouse gas concentrations and radiative forcing, a detailed understanding of differences in biogeochemical cycling between modern and ancient marine environments is required. In the oxygen minimum zones of upwelling areas in the modern ocean, organic matter decomposition is mediated by denitrification (Gruber and Sarmiento, 1997), which is why these systems are classified as nitrogenous. By contrast, the notion of nitrogenous conditions at anoxic continental margins is rarely championed in pre-Cenozoic Earth history. Many studies have reported proxy evidence for anoxic and sulfidic (typically referred to as euxinic) conditions in the context of Mesozoic and Paleozoic OAEs (Meyer and Kump, 2008). Under euxinic conditions, bacterial sulfate reduction dominates organic matter decomposition in the water column. In many cases, euxinic conditions extended into the photic zone (sunlit surface ocean), as revealed by the presence of biomarkers related to green sulfur bacteria (anaerobic phototrophs)

(Sinninghe Damsté and Kösters, 1998; Kolonic et al., 2005). In the modern ocean euxinic conditions are restricted to semi-enclosed basins such as the Black Sea, Cariaco Basin and Baltic Sea Deeps. Due to the lack of upwelling in these density-stratified epeiric basins, euxinic conditions are limited to the subsurface and generally do not expand into the photic zone. A third mode of ocean anoxia, ferruginous conditions, was originally assigned to the sulfate- and thus sulfide-poor ocean in the Precambrian, but does not exist in the ocean today. Under ferruginous conditions, hydrogen sulfide (H_2S) accumulation is prevented by a surplus of Fe minerals ((oxyhydr)oxides and carbonates) that are reactive towards H_2S. Due to quantitative precipitation of H_2S as Fe sulfide mineral, dissolved Fe (Fe^{2+}) can become the dominant redox species in the anoxic water column (Poulton and Canfield, 2011). Recently, an increasing number of paleo-studies have reported proxy-based evidence for ferruginous conditions along anoxic continental margins in the Phanerozoic ranging from the Eocene back to the Permian (e.g., März et al., 2008; Dickson et al., 2014; Poulton et al., 2015; Clarkson et al., 2016).

Based on the apparent "chronosequence" of redox conditions along anoxic ocean margins described above, it could be inferred that the ocean underwent a progressive transition from predominantly ferruginous or euxinic to nitrogenous anoxia over the course of Earth history. On the other hand, sedimentary proxies for iron and sulfur cycling (e.g., Fe speciation, sulfur isotopes, molybdenum (Mo) concentrations and isotopes) are rarely combined with proxies for nitrogen cycling (nitrogen isotopes) and the mechanisms leading to a transition from nitrogenous to euxinic or ferruginous conditions (or vice versa) are poorly constrained. As a consequence, the application of biogeochemical concepts established in the context of Earth system perturbations in the geological past to current and future environmental change is problematic.

To address this issue, we compare proxy records of coupled biogeochemical cycling of Fe, sulfur and nitrogen in the Tarfaya upwelling system of the Proto-North Atlantic during the Cenomanian-Turonian with proxy data for modern upwelling-related oxygen minimum zones. The overarching objectives of this study are:

1. Determine the redox structure at the southeastern margin of the Proto-North Atlantic before, during and after the Cenomanian-Turonian OAE2 (~94 - 93 Ma).

2. Evaluate proxy-based evidence for transitions from nitrogenous to ferruginous to euxinic conditions in the Tarfaya upwelling region over these time intervals.

3. Explore mechanisms that facilitated the onset of permanently euxinic conditions in Cretaceous upwelling systems compared to the modern ocean.

2. Environmental setting

Due to intense terrestrial and submarine volcanic activity, CO_2 concentrations in the atmosphere were considerably higher (~500 - 1300 ppmv) in the middle to late Cretaceous compared to the pre-industrial level of 280 ppmv (Arthur et al., 1985; Berner, 2006; Royer et al., 2014; Wang et al., 2014). As a consequence of high CO_2 concentrations and globally elevated temperatures, the Earth was essentially ice-free and latitudinal temperature gradients were greatly reduced (Hay et al., 2008).

Our study area, the Proto-North Atlantic (Fig. 1A), was smaller than its present-day counterpart (Fig. 1B) and separated from adjacent ocean basins by sills and narrow seaways. Because of restricted connections and an estuarine circulation pattern, the Proto-North Atlantic was prone to sluggish deep-water renewal and anoxia (Trabucho Alexandre et al., 2010; Monteiro et al., 2012). Global Climate Models (Trabucho Alexandre et al., 2010) and micropaleontological data (Einsele and Wiedmann, 1982; Kuhnt et al., 1997) suggested that the northwest African margin in the southeastern Proto-North Atlantic hosted a productive coastal upwelling system, similar to those off the coasts of Peru and Namibia today. In the Tarfaya Basin in southern Morocco, a >700 m thick sedimentary succession of Upper Cretaceous organic carbon-rich and partly laminated marls, shales and limestones provides evidence of this ancient upwelling system (Kuhnt et al., 2001). Considering its spatial extent and the high organic carbon mass accumulation rates, the Tarfaya Basin represented a carbon sink of global significance (Kolonic et al., 2005).

We focus here on drill core Tarfaya SN4, which was recovered ~37 km east of the town of Tarfaya in December 2009 (Kuhnt et al., 2017). During the Cenomanian-Turonian, this site was located in an outer shelf setting at 200 to 300 m water depth. A total of 350 m of sedimentary rocks were drilled corresponding approximately to 5 million years of sedimentation between the latest Albian and early Turonian (Beil et al., 2018). Oceanic Anoxic Event 2, as identified by a positive organic carbon isotope ($\delta^{13}C_{org}$) excursion at a downcore depth of 80 to 110 m (Fig. 2), corresponds to a succession of organic-rich black shales and marls (Kuhnt et al., 2017). The $\delta^{13}C_{org}$ excursion is typical for OAE sediments worldwide and related to globally elevated rates of organic carbon burial (e.g., Jenkyns, 2010). A transient shift towards lower $\delta^{13}C_{org}$ values following the first increase at the onset of OAE2 (~101 m) (Fig. 2B) is attributed to a short-lived period of global cooling, the so-called "Plenus Cold Event" (PCE) (Kuhnt et al., 2017). Average sedimentation rates increased from 4.5 cm/kyr to 7.7 cm/kyr at 120 m depth (Kuhnt et al., 2017).

Previous work at multiple sites within the Tarfaya Basin revealed that sedimentation rates generally increase from near-shore to outer shelf locations, from Mohammed Plage to core S75, core S57 and core S13 (Fig. 1C) (Kuhnt et al., 1997; Kolonic et al., 2005). Site SN4 is located close to the outer shelf depocenter (Fig. 1C), where the highest sedimentation and organic carbon mass accumulation rates prevailed. A previous study on water column biogeochemical cycling within the Tarfaya Basin during OAE2 reported organic geochemical evidence for euxinic conditions, sometimes extending into the photic zone (Kolonic et al., 2005). These findings were later corroborated by Poulton et al. (2015), whose sedimentary Fe speciation data for core S57 are consistent with sustained periods of euxinic conditions during OAE2. In addition, these authors reported occasional excursions towards ferruginous conditions (Fe > H_2S in the water column). A drawdown of the oceanic sulfate inventory could be ruled out based on sulfur isotope data. The occurrence of ferruginous conditions was instead attributed to enhanced Fe supply from the adjacent continent (Poulton et al., 2015). Core S57 is located approximately 15 km further onshore and at somewhat shallower water depth than SN4 (Fig. 1C). By comparing proxies for Fe and sulfur cycling at these two

locations, we can derive information about lateral gradients in redox conditions and element turnover across the Cretaceous upwelling system. Moreover, since the sedimentary succession in core SN4 starts more than 4 million years prior to the onset of OAE2, we can provide new constraints on how redox conditions in the upwelling system evolved since the Albian-Cenomanian transition.

3. Methods

Samples for this study were taken from the archived core SN4 in 2016 with an average resolution of 2.4 $\pm$ 0.8 m (1 SD, n = 109). Sample intervals were chosen based on the high-resolution $\delta^{13}C_{org}$ record (Fig. 2) published by Kuhnt et al. (2017) and Beil et al. (2018). To prevent sampling of oxidized or contaminated material, the surface of the samples was scraped off using a titanium knife. The remaining material was crushed and ground using a mortar and agate mill. Total organic carbon (TOC) and total nitrogen (TN) concentrations were determined with an element analyzer (Euro EA, HEKAtech). Bulk sedimentary nitrogen isotope ratios were determined using an elemental-analysis isotope-ratio mass spectrometer (EA-IRMS, INTEGRA2, Sercon Limited). Ratios of ^{15}N to ^{14}N are reported in conventional delta-notation with respect to atmospheric N_2 (AIR) after calibration with internal and international standards (IAEA-N1 and IAEA-N2). The Analytical reproducibility of replicate samples and standard measurements was generally better than ± 0.15 ‰ (1 SD).

For the analysis of total element concentrations, sediment samples were digested with hydrofluoric acid (40 % trace metal clean), nitric acid (65 % sub-boiled-distilled) and perchloric acid (60 %, pro analysis) on a hotplate. After evaporation of the acid mix and re-dissolution in dilute nitric acid, the samples were analyzed for major and trace element concentrations by inductively coupled plasma optical emission spectrometry (ICP-OES, VARIAN 720-ES) and mass spectrometry (ICP-MS, Agilent Technologies 7500 Series). To monitor the accuracy and precision of the whole procedure, method blanks and the reference standards MESS-3 (marine sediment, Canadian Research Council) SDO-1 (Devonian Ohio Shale, USGS) and SCo-1 (Cody Shale, USGS) were digested and analyzed along with samples. Analyte concentrations were generally within the certified ranges and replicate

digestions yielded relative standard deviations of less than 2 %. To illustrate enrichments or depletions relative to the lithogenic background, Fe concentrations are normalized to aluminum (Al) and compared to the metal/Al of the upper continental crust (UCC) (Fe/Al = 0.44) (McLennan, 2001). Similarly, Mo and vanadium (V) concentrations are reported as excess concentrations above UCC (V/Al = $1.33 \cdot 10^{-3}$; Mo/Al = $1.87 \cdot 10^{-5}$) (McLennan, 2001): $Metal_{XS} = Metal_{sample} - (Metal/Al)_{crust} \cdot Al_{sample}$.

A sequential extraction scheme was applied to determine operationally defined pools of reactive Fe minerals in sediment samples (Poulton and Canfield, 2005). In brief, Fe bound to carbonate minerals (Fe_{carb}) was extracted with sodium acetate, Fe bound to (oxyhydr)oxide minerals (Fe_{ox}) was extracted with sodium dithionite and magnetite Fe (Fe_{mag}) was extracted with ammonium oxalate. Extraction solutions were analyzed for Fe concentration by ICP-OES. Concentrations of Fe bound to pyrite (Fe_{py}) were determined by the chromium reduction method (Canfield et al., 1986). The sum of these four fractions represents the highly reactive Fe pool (Fe_{HR}) which can be compared to the total Fe concentration (Fe_T) obtained by total digestion. The accuracy and precision of the procedure were determined by extracting various shales from the United Kingdom within the framework of an interlaboratory comparison led by S. Poulton (University of Leeds).

4. Results and discussion

4.1. Iron speciation across the southeastern margin of the Proto-North-Atlantic

In core SN4, the ratios of highly reactive Fe to total Fe (Fe_{HR}/Fe_T) (Fig. 2) are generally elevated above the commonly applied threshold for anoxic conditions ($Fe_{HR}/Fe_T > 0.38$) (Poulton and Canfield, 2011). The extent to which highly reactive Fe minerals have been converted to pyrite (Fe_{py}/Fe_{HR}) (Fig. 3) remains below the typical threshold for euxinic conditions of 0.7 - 0.8 (Poulton and Canfield, 2011). This combination of Fe speciation proxies suggests that the water column was characterized by anoxic and non-sulfidic (so-called ferruginous) conditions throughout the time period represented by core SN4. This observation contrasts with previously reported Fe speciation data from core S57 covering the onset of OAE2, which mostly indicate euxinic conditions and revealed only occasional

excursions towards anoxic and non-sulfidic conditions in the water column (Fig. 3) (Poulton et al., 2015). Iron speciation data for the deep Proto-North Atlantic at DSDP Site 367 (>2000 m water depth) (Fig. 1A) pointed to anoxic and non-sulfidic conditions prior to OAE2 and mostly euxinic conditions during OAE2 (Fig. 3) (Westermann et al., 2014). Taken together, the previously published and our new Fe speciation data suggest that during OAE2 mostly euxinic deep and (sub)surface waters were separated by constantly ferruginous intermediate waters, which occasionally expanded to shallower water depth. We argue, however, that such a water-mass structure is not plausible and that the Fe speciation data from the Tarfaya Basin cannot be interpreted in this way.

Core SN4 (this study) and S57 (investigated by Poulton et al., 2015) are only ~15 km apart (Fig. 1C). Using the averaged global shelf geometry of the modern ocean, this distance translates into an approximate depth difference of only 25 m. Taking into account that the average modern shelf geometry is based on both passive (as for Tarfaya) and steeper active margins and that shelf areas were more expanded during the Late Cretaceous (Bjerrum et al., 2006), the depth difference between the two cores was likely even smaller. Over such a short vertical distance, a water column redox boundary that is largely stable over hundreds of thousands of years, despite sea level fluctuations (Beil et al., 2018), is unlikely to have become established. Similar spatial transitions from intermediate to high Fe_{py}/Fe_{HR} have been reported for modern productive continental margins such as the Peru upwelling system (Scholz et al., 2014). However, increasing Fe_{py}/Fe_{HR} in a shoreward direction within this system is not related to a transition from non-euxinic to euxinic conditions in the overlying water column, but rather to a lateral gradient in the rates of primary production, organic carbon rain and anaerobic microbial metabolism (Dale et al., 2015).

In the lower section of core SN4 (lower Cenomanian, depth of ~300 - 230 m), Fe_{HR}/Fe_T ratios are generally elevated above the threshold for anoxia (0.51 ± 0.14, n = 17). However, the corresponding sediments are only moderately enriched in organic carbon (<2 wt.% on average) and are devoid of the redox-sensitive trace metals V and Mo, which would be expected to accumulate in an anoxic ocean region (Fig. 2A) (Brumsack, 2006). This contradiction suggests that Fe speciation proxies in

sediments of the Tarfaya basin have to be interpreted with respect to environmental factors other than redox conditions.

4.2. Significance of the ferruginous proxy signature

The solubility of Fe in anoxic seawater is generally enhanced compared to oxic seawater. Therefore, dissolved Fe from sedimentary Fe release or hydrothermal sources can be efficiently transported in anoxic ocean regions. Once the dissolved Fe is transferred into an area with oxic or strongly sulfidic conditions in the water column, the capacity for Fe transport is markedly lowered because authigenic Fe minerals (oxides, sulfides or carbonates) are precipitated and deposited at the seafloor. Under such conditions, the accumulation of reactive Fe is decoupled from the terrigenous Fe input, thus leading to elevated ratios of Fe_{HR} to Fe_T and high Fe_T contents relative to Al compared to terrigenous particles and sediments that are unaffected by Fe precipitation in the water column (Lyons and Severmann, 2006; Poulton and Canfield, 2011). The two ratios (Fe_{HR}/Fe_T and Fe_T/Al) will respond in a predictable manner to the addition of non-terrigenous reactive Fe, which can be calculated using the following set of equations (Scholz et al., 2018):

$$Fe_T/Al = \frac{MAR \cdot Al \cdot \left(\frac{Fe_T}{Al}\right)_{in} + (RR_{Fe} \cdot M_{Fe})}{MAR \cdot Al} \quad (1)$$

$$Fe_{HR}/Fe_T = \frac{MAR \cdot Al \cdot \left(\frac{Fe_T}{Al}\right)_{in} \cdot \left(\frac{Fe_{HR}}{Fe_T}\right)_{in} + (RR_{Fe} \cdot M_{Fe})}{MAR \cdot Al \cdot \left(\frac{Fe_T}{Al}\right)_{in} + (RR_{Fe} \cdot M_{Fe})} \quad (2)$$

In these equations, MAR is the sediment mass accumulation rate (in g cm^{-2} yr^{-1}), Al is the aluminum concentration (in mg g^{-1}), $(Fe_T/Al)_{in}$ and $(Fe_{HR}/Fe_T)_{in}$ are the initial ratios prior to deposition of excess reactive Fe (i.e., corresponding to the terrigenous input), RR_{Fe} is the rain rate of non-terrigenous reactive Fe (in mmol cm^{-2} yr^{-1}) and M_{Fe} is the molar mass of Fe (55.845 mg $mmol^{-1}$).

Adopting a range of RR_{Fe} yields a trend line of Fe_T/Al versus Fe_{HR}/Fe_T (Fig. 4A), which can be used to evaluate whether a measured Fe proxy signature can be assigned to a net transfer of reactive Fe into an anoxic ocean region (see Scholz et al. (2018) for further details). Importantly, the shape of the trend line and its position within the Fe_T/Al versus Fe_{HR}/Fe_T space solely depends on $(Fe_T/Al)_{in}$ and $(Fe_{HR}/Fe_T)_{in}$ but are unaffected by MAR, Al and RR_{Fe}.

The use of Fe_{HR}/Fe_T and Fe_T/Al as redox proxies is based on the notion that reactive Fe minerals that precipitate in the water column are mixed with sediments whose Fe content is determined by terrigenous input. In a first modeling approach we therefore use the Fe_T/Al of UCC (Fe_T/Al = 0.44) (McLennan, 2001) and Fe_{HR}/Fe_T of modern continental margin sediments with oxic bottom water (Fe_{HR}/Fe_T = 0.28) (a compilation of data for sediments from Long Island Sound, Baltic Sea, Mississippi Delta and NW Mediterranean Sea) (Raiswell and Canfield, 1998) as initial values. Most of the data from the Tarfaya Basin and deep Proto-North Atlantic do not plot on the corresponding trend line but are shifted towards higher Fe_{HR}/Fe_T. In theory, a shift into this direction could be generated through pyritization of Fe bound to silicate minerals (Scholz et al., 2018), e.g., due to long-term exposure of clay minerals to H_2S (Raiswell and Canfield, 1996). However, given that the extent to which reactive Fe minerals have undergone pyritization in core SN4 is far from unity (Fe_{py}/Fe_{HR} = 1) (Fig. 2), it is unlikely that appreciable amounts of less reactive Fe in silicate minerals were converted to pyrite. We therefore conclude that the Fe_{HR}/Fe_T and Fe_T/Al of modern continental margin sediments with oxic bottom water and UCC do not represent appropriate initial values for the sediments from the Proto-North Atlantic.

In order to fit Equations (1) and (2) to the range of Fe_{HR}/Fe_T and Fe_T/Al reported from the Cenomanian-Turonian Proto-North Atlantic, a variety of initial values for Fe_{HR}/Fe_T are required (Fig. 4A). These terrigenous input values are mostly higher than the commonly applied threshold for anoxic conditions (Fe_{HR}/Fe_T = 0.38), suggesting that much of the reactive Fe enrichment may not be related to water column redox conditions but to a differing terrigenous input to the Proto-North

Atlantic compared to the present-day. Reactive Fe is generated during weathering on land through transformation of ferrous Fe in silicate minerals to ferric Fe (oxyhydr)oxides. As weathering progresses, silica and soluble cations are lost to solution, which is why Fe_{HR}/Fe_T and, to a lesser extent, Fe_T/Al increase (Schwertmann, 1988). The Fe_{HR}/Fe_T of modern continental margin sediments with oxic bottom water (Fe_{HR}/Fe_T = 0.28) corresponds to a moderate weathering intensity, which is typical for soils in a temperate climate regime (Blume, 1988). In contrast, in a warm and humid sub-tropical to tropical climate, the process of silicate weathering may proceed to near-completion, thus, leading to the formation of saprolite and laterite. These weathering assemblages consist almost exclusively of kaolinite and/or Fe and Al (oxyhydr)oxides and their Fe_{HR}/Fe_T approaches unity (Widdowson, 2007). An important pre-requisite for the formation of Fe-rich weathering assemblages is a relatively quiescent tectonic regime so that intense and deep-reaching weathering is not prevented by uplift and, thus, erosion of immature weathering products (Widdowson, 2007).

In the Late Cretaceous greenhouse climate (Arthur et al., 1985; Hay, 2008), tropical weathering was more prevalent compared to the present-day (Widdowson, 2007; Craggs et al., 2012; Bata et al., 2016). Moreover, the Cretaceous land surfaces were characterized by shallow relief (Hay et al., 2019). Therefore, erosion and sediment transport to the ocean were reduced compared to the late Cenozoic (Ronov, 1994; Royer et al., 2014). Overall, these conditions were highly conducive to transport-limited weathering and a higher proportion of reactive Fe in the terrigenous material transported to the ocean. To evaluate the impact of intensified terrigenous weathering on Fe speciation (i.e., Fe_T/Al and Fe_{HR}/Fe_T) in continental margin sediments, we calculate mixing arrays between UCC/modern continental margin sediments with oxic bottom water and the range of data covered by laterite profiles in India (on Late Cretaceous Deccan basalt and Proterozoic greywacke) (Widdowson, 2007) (Fig. 4B):

$$Fe_T/Al = \frac{f_{mod} \cdot Al_{mod} \cdot \left(\frac{Fe_T}{Al}\right)_{UCC} + f_{lat} \cdot Al_{lat} \cdot \left(\frac{Fe_T}{Al}\right)_{lat}}{f_{mod} \cdot Al_{mod} + f_{lat} \cdot Al_{lat}} \quad (3)$$

$$Fe_{HR}/Fe_T = \frac{f_{mod} \cdot Al_{mod} \cdot \left(\frac{Fe_T}{Al}\right)_{UCC} \cdot \left(\frac{Fe_{HR}}{Fe_T}\right)_{mod} + f_{lat} \cdot Al_{lat} \cdot \left(\frac{Fe_T}{Al}\right)_{lat} \cdot \left(\frac{Fe_{HR}}{Fe_T}\right)_{lat}}{f_{mod} \cdot Al_{mod} \cdot \left(\frac{Fe_T}{Al}\right)_{UCC} + f_{lat} \cdot Al_{lat} \cdot \left(\frac{Fe_T}{Al}\right)_{UCC}}$$

(4)

In these equations, indices 'UCC', 'mod' and 'lat' refer to upper continental crust, modern continental margin sediments with oxic bottom water and laterite, respectively. Mixing proportions between zero and one are represented by f_{mod} and f_{lat} ($f_{mod} + f_{lat} = 1$).

The mixing arrays in Fig. 4B reveal that most of the Fe speciation data from the Proto-North Atlantic can be generated by mixing modern continental margin sediments with a tropical weathering assemblage. Intense continental weathering is plausible explanation for elevated Fe_{HR}/Fe_T and Fe_T/Al in the lower part of the SN4 record (~300 - 230 m), where a lack of trace metal enrichment and low TOC concentrations (Fig. 2) are indicative of oxic bottom waters at the time of deposition. Above a downcore depth of 230 m, oxygen-deficient conditions in the bottom water are supported by elevated TOC concentrations and sedimentary V and Mo enrichments (Fig. 2A). Under these conditions, dissolved Fe transport and precipitation in the water column may have contributed to reactive Fe enrichments. However, the shift in baseline Fe_{HR}/Fe_T compared to modern continental margin sediments needs to be taken into account when applying a Fe_{HR}/Fe_T threshold for anoxic conditions. Moreover, in the Late Cretaceous generating elevated Fe_{HR}/Fe_T was likely facilitated by lower rates of terrigenous sedimentation compared to the late Cenozoic (Ronov, 1994; Royer et al., 2014). While sedimentary Fe_{HR}/Fe_T in cores from the Tarfaya upwelling area are elevated compared to those of modern upwelling system, the total Fe and Al concentrations and corresponding mass accumulation rates are comparably low (Table 1). A moderate shift in Fe_{HR}/Fe_T from 0.51 $\pm$ 0.14 (n = 17) below 230 m to 0.73 $\pm$ 0.15 (n = 54) above this depth could, thus, be mediated by a relatively small additional flux of authigenic Fe (Scholz et al, 2018). The effect of authigenic Fe supply on Fe_{HR}/Fe_T as a function of differing rates of terrigenous background sedimentation is illustrated in Fig. 5. Due to low rates of terrigenous Fe and Al accumulation in the Tarfaya Basin, the Fe_{HR}/Fe_T was more

sensitive towards authigenic Fe supply compared to modern continental margin settings such as the Peru margin, where terrigenous sedimentation is higher (Fig. 5). In fact, the difference in Fe_{HR}/Fe_T between the lower Cenomanian and upper Cenomanian/Turonian sediments in Tarfaya on one side and UCC/modern continental margin sediments with oxic bottom water and Peru margin shelf sediments on the other side can be explained by the same authigenic Fe rain rate of 1.0 µmol cm^{-2} yr^{-1} (Fig. 5). In other words, the quantitative Fe speciation approach adopted here reveals that the amount of dissolved Fe transported and precipitated per unit time in the water column of the Tarfaya upwelling system was similar to that in modern upwelling systems, such as the Peruvian continental margin.

The comparably low mass accumulation rates of total Fe and reactive Fe in the Tarfaya upwelling system (Table 1) have important implications for the interpretation of Fe_{py}/Fe_{HR}. At a high accumulation rate of organic material (fueling bacterial sulfate reduction and H_2S production), in concert with a lower accumulation rate of Fe_{HR}, quantitative pyritization is more readily achieved than in a scenario where both organic material and Fe_{HR} accumulate at high rates. Sediments in the Tarfaya upwelling system during OAE2 and on the Peru margin are characterized by similar Fe_{py}/Fe_{HR} (Fig. 3) (Poulton et al., 2015) and TOC accumulation rates (Table 1). By contrast, Fe_{HR} mass accumulation rates on the Peruvian margin are at least twice as high as in the Tarfaya system. This observation implies that the total amount of H_2S available for pyritization (i.e., in the water column and sediments) in the Tarfaya upwelling system was smaller than that on the Peruvian continental margin today, where most of the time sulfidic conditions are limited to the sediment pore water.

4.3. Nitrogen cycling as a key-control on water column redox conditions

The lower dissolved Fe or H_2S concentrations in the Tarfaya upwelling system compared to modern upwelling systems such as the Peruvian margin are in seeming contrast to organic geochemical studies in the Tarfaya Basin, which demonstrated the occurrence of biomarkers that are indicative of green sulfur bacteria and, thus, H_2S in the photic zone during OAE2 (Sinninghe Damsté

and Kösters, 1998; Kolonic et al., 2005). At continental margins strongly reducing conditions are generally expected to emerge from seafloor sediments, where ferruginous and sulfidic conditions are first established. At most productive continental margins in the modern ocean, H_2S release from the sediment to the water column is generally inhibited by chemolithoautotrophic sulfide oxidation with nitrate in the bottom water and surface sediment (Fossing et al., 1995; Schulz et al., 1999). Similarly, sedimentary Fe release has been proposed to be limited by nitrate-dependent Fe oxidation (Scholz et al., 2016). However, during times of high productivity and water column stagnation bottom waters can become nitrate- and nitrite-depleted through quantitative denitrification and anammox. Under such conditions sedimentary sulfide release and moderate sulfide concentrations in the water column (tens of µM) can be observed, e.g., in the upwelling areas off Namibia (Brüchert et al., 2003) and Peru (Schunck et al., 2013; Scholz et al., 2016). Taking these modern upwelling environments as analogues, we suggest that nitrogen cycling played a key role in determining water column redox conditions in the Tarfaya upwelling system and we substantiate this view using nitrogen isotope systematics.

Cretaceous sediments are characterized by low nitrogen isotope values (average $\delta^{15}N \approx -2$ ‰) (Fig. 2) compared to modern marine sediments (average $\delta^{15}N \approx +5$ ‰) (Algeo et al., 2014). Sedimentary $\delta^{15}N$ generally reflects the isotope composition of primary producers. Phytoplankton organisms incorporate the $\delta^{15}N$ of the fixed nitrogen, which, on a global scale, is controlled by the balance between nitrogen fixation and nitrogen loss by partial pelagic versus near-quantitative benthic denitrification (Brandes and Devol, 2002). According to Algeo et al. (2014), greatly expanded shelf areas in the Cretaceous (Bjerrum et al., 2006) favored more widespread benthic denitrification, which is near-quantitative and, therefore, has a negligible isotope effect compared to partial pelagic denitrification (Sigman et al., 2003; Lehmann et al., 2004). As a consequence, the $\delta^{15}N$ of the fixed nitrogen pool was shifted more towards the isotope composition of newly fixed nitrogen (i.e., $\delta^{15}N$ around 0 ‰). In addition, quantitative pelagic denitrification under euxinic conditions coupled to

upwelling and partial assimilation of ammonia has been invoked to explain sedimentary $\delta^{15}N$ below 0 ‰ during OAEs (Junium and Arthur, 2007; Higgins et al., 2012).

More quantitative denitrification and widespread nitrogen fixation, implied by generally low Cretaceous sedimentary $\delta^{15}N$, suggest that the overall nitrate inventory of the Cretaceous ocean was considerably smaller compared to that of the present-day (Junium and Arthur, 2007). Under such conditions, a complete nitrate drawdown in the nitrogenous zones of reducing ocean margins and subsequent sedimentary sulfide and Fe release could be achieved at substantially lower rates of export production than in the modern ocean, which is nitrate-replete. According to this view, the presence of biomarker evidence for photic zone euxinia is not necessarily indicative of intense H_2S generation in the water column but rather of lower nitrate concentrations and reduced oxidation of sediment-derived sulfide. Considering the low reactive Fe mass accumulation rates as well as moderate Fe_{py}/Fe_{HR} and TOC mass accumulation rates in the Tarfaya sediments (Table 1, Fig. 2 and 3), H_2S concentrations in the water column were probably low and similar to those observed during sulfidic events in modern upwelling areas (tens of µM), yet far from the H_2S concentrations in the euxinic Black Sea (hundreds of µM) (Scholz et al., 2018).

4.4. Evolution of water column redox conditions across OAE2

Lower to middle Cenomanian sediments are characterized by low concentrations of organic carbon and redox-sensitive metals as well as low Fe_{py}/Fe_{HR} (Fig. 2A). This combination of biogeochemical proxies is indicative of oxic conditions in the bottom water at the time of deposition. Sediments at the Albian-Cenomanian boundary feature the lowest $\delta^{15}N$ values (~-2.5 ‰) within the entire SN4 record. Previous studies attributed similarly low $\delta^{15}N$ values during OAE2 to upwelling of ammonia with anoxic subsurface waters and partial ammonia assimilation in the photic zone (Junium and Arthur, 2007; Higgins et al., 2012). Such a scenario can be ruled out for the Tarfaya system at the Albian-Cenomanian boundary, since all available proxies indicate oxic conditions in the bottom water well below the surface. Any ammonia released during organic matter remineralization would be

readily oxidized prior to reaching the surface ocean under such conditions. Zhang et al. (2014) suggested that $\delta^{15}N \leq 2.5$ ‰ during Cretaceous OAEs may reflect the use of alternative enzymes (i.e., nitrogenases with Fe or V instead of Mo as a co-factor) by nitrogen-fixing phytoplankton in response to global drawdown of Mo under widespread euxinic conditions. While we cannot exclude this scenario, it is counterintuitive to assume a global Mo drawdown during times of oxic conditions and negligible Mo accumulation in the Tarfaya Basin. An alternative explanation for low $\delta^{15}N$ could be incomplete nitrate utilization under conditions where primary production is limited by P or Fe rather than fixed nitrogen (Altabet and Francois, 1994). Such a scenario would be consistent with the low terrigenous input (Table 1) and oxic conditions in the bottom water, which prevent any P and Fe supply from reducing sediments (Scholz et al., 2018).

During the middle Cenomanian and thereafter (above ~230 m downcore depth) generally increasing Fe_{HR}/Fe_T, Fe_{py}/Fe_{HR} and concentrations of TOC, V and Mo (Fig. 2A) indicate oxygen-deficient conditions in the bottom water. These trends support earlier findings, suggesting that the transition towards an oxygen-depleted upwelling system proceeded in multiple steps, one of which took place during the mid-Cenomanian (Beil et al., 2018). The onset of oxygen-deficient conditions coincides with a rise in $\delta^{15}N$ from -2.5 ‰ at the Albian-Cenomanian boundary (~300 m) to ~0 ‰ at 130 m downcore depth. Coeval V and Mo concentration levels and ratios (Fig. 2A) as well as Fe speciation signatures (Fig. 3 and 5, Table 1) are fully consistent with biogeochemical cycling in modern upwelling-related oxygen minimum zones (Scholz et al., 2018), where denitrification takes place in the water column. As a consequence, we attribute the increase in $\delta^{15}N$ to partial denitrification of upwelled nitrate in an oxygen-depleted water column. Against the backdrop of low global seawater $\delta^{15}N$ in the Cretaceous, partial denitrification still yielded a lower sedimentary $\delta^{15}N$ compared to modern oxygen minimum zones. Importantly, however, the relative shift in $\delta^{15}N$ of +2.5 ‰ between continental margin settings with and without water column denitrification is comparable to the modern ocean (e.g., Mollier-Vogel et al., 2012). In addition, sedimentary P and Fe release

under oxygen minimum zone-like conditions (Scholz et al., 2018) may have mitigated Fe and P limitation, and may thus have contributed to the rise in $\delta^{15}N$.

Above 130 m downcore depth, $\delta^{15}N$ decreases again and reaches minimum values of -1.5 ‰ at the beginning of the $\delta^{13}C_{org}$ excursion that is associated with the onset of OAE2 (Fig. 2B). Iron speciation proxies as well as trace metal and organic carbon concentrations remain elevated throughout most of this interval. Therefore, a return towards well-oxygenated conditions such as at the Albian-Cenomanian boundary can be excluded to explain decreasing $\delta^{15}N$. Upwelling and partial assimilation of ammonia under euxinic conditions (Junium and Arthur, 2007; Higgins et al., 2012) or a switch towards the use of alternative nitrogenases due to changes in the trace metal stoichiometry of seawater (Zhang et al., 2014) are plausible explanations for the $\delta^{15}N$ decrease during the transition into OAE2. In any case, the onset of anoxic and euxinic conditions in the Tarfaya upwelling system, as indicated by organic geochemical evidence for photic zone euxinia during OAE2 (Sinninghe Damsté and Kösters, 1998; Kolonic et al., 2005), required a quantitative nitrate drawdown by denitrification (see previous section) and, thus, a return towards low $\delta^{15}N$.

Above ~115 m downcore depth, Mo and, to a lesser extent, V concentrations decrease while organic carbon concentrations as well as Fe_{HR}/Fe_T and Fe_{py}/Fe_{HR} remain elevated (Fig. 2B). Decreasing accumulation rates of redox-sensitive metals at the onset of OAE2 reported by previous studies were commonly assigned to large-scale burial of these elements (especially Mo) in anoxic ocean regions and an associated drawdown of the global ocean's trace metal inventories (Dickson et al., 2016; Owens et al., 2016). A concomitant shift towards higher V to Mo ratios ($(V/Mo)_{XS}$) (Fig. 2B) may reflect changes in the trace metal stoichiometry of seawater, which could have provoked a switch towards the use of alternative nitrogenases. Muted trace metal accumulation persisted throughout the onset of OAE2 and until the PCE, a global cooling event that was possibly related to large-scale organic carbon burial and the associated drawdown of CO_2 from the atmosphere (Jenkyns et al., 2017; Kuhnt et al., 2017). Uranium isotope variability across OAE2 suggests that the PCE coincided with a transient episode of global re-oxygenation (Clarkson et al., 2018). In agreement with this

notion, our $\delta^{15}N$ record is consistent with a transient return towards nitrogenous and, thus, non-euxinic conditions in the Tarfaya upwelling system during the PCE (Fig. 2B). Less reducing conditions likely mediated a recovery of the oceanic trace metal inventories (Jenkyns et al., 2017), which is reflected by the return to high trace metal accumulation rates after the PCE (Fig. 2B).

Previous studies reported thallium isotope evidence for globally reduced manganese oxide burial and, by inference, ocean deoxygenation about 50,000 years prior to OAE2 (Ostrander et al., 2017). In core SN4 the depth difference between the first drop in $\delta^{15}N$ above 130 m or trace metal concentrations at ~115 m and the onset of OAE2 (~107 m) (Fig. 2B) corresponds to a period of ~400,000 ($\delta^{15}N$) and ~115,000 (V and Mo) years. This time lag reveals that the intensification of reducing conditions and associated transitions in biogeochemical cycling in the Tarfaya upwelling system initiated even longer before the global anoxic event.

5. Summary and implications

Our novel quantitative approach to sedimentary Fe speciation suggests that elevated Fe_{HR}/Fe_T and Fe_T/Al in the Proto-North Atlantic were, to a large part, related to transport-limited chemical weathering in the Cretaceous greenhouse climate rather than Fe precipitation from anoxic seawater. Transport-limited weathering implies a reduced flux of terrigenous material that is, however, more intensely weathered and, thus, enriched in Fe (oxyhydr)oxides. Because of low terrigenous sedimentation rates in the late Cretaceous in general (Ronov, 1994), and the Tarfaya Basin in particular, the overall mass accumulation rates of total Fe and reactive Fe were low compared to modern upwelling regions. As a result, a relatively low authigenic Fe rain rate and a moderate sulfate reduction rate could result in a Fe_{HR}/Fe_T and Fe_{py}/Fe_{HR} signature, which would commonly be assigned to ferruginous anoxia. However, by unraveling the effect of intensified chemical weathering and reduced terrigenous sedimentation on Fe speciation proxies, we demonstrate that the biogeochemical cycles of Fe and sulfur operated remarkably similar to the ones in modern oxygen minimum zones.

Chemical weathering on land and terrigenous sedimentation fluctuated considerably over the course of Earth's history (Ronov, 1994; Royer et al., 2014). Both these processes strongly impact the amount of authigenic Fe that is required to generate Fe_{HR}/Fe_T and Fe_{py}/Fe_{HR} above the typical threshold values for anoxic and euxinic or ferruginous conditions and need, therefore, be considered when interpreting Fe-based paleo-redox proxies. The term "ferruginous" is widely used in studies on biogeochemical cycling in deep time. However, as demonstrated here and by previous work (Scholz et al., 2018), a ferruginous proxy signature, water column denitrification and (low) sulfide or even oxygen concentrations in the water column are not mutually exclusive. We argue that a biogeochemically more consistent definition of "ferruginous anoxia" is required to apply biogeochemical concepts that were established in the context of OAEs to present or future environmental change.

Acknowledgements

We would like to thank Anna-Kathrin Retschko, Regina Surberg, Thomas Kuhn and Bettina Domeyer for laboratory assistance. This work was supported by the German Research Foundation (DFG) through Emmy Noether Research Group ICONOX (Iron Cycling in Continental Margin Sediments and the Nutrient and Oxygen Balance of the Ocean) and Subproject A7 of the Collaborative Research Centre 754 (Climate-Biogeochemistry Interactions in the Tropical Ocean). Constructive comments by Jeremy Owens and an anonymous reviewer are gratefully acknowledged.

References

Algeo, T.J., Meyers, P.A., Robinson, R.S., Rowe, H., Jiang, G.Q., 2014. Icehouse-greenhouse variations in marine denitrification. Biogeosciences 11, 1273-1295.

Altabet, M.A., Francois, R., 1994. Sedimentary nitrogen isotopic ratio as a recorder for surface ocean nitrate utilization. Global Biogeochemical Cycles 8, 103-116.

Arthur, M.A., Dean, W.E., Schlanger, S.O., 1985. Variations in the Global Carbon Cycle During the Cretaceous Related to Climate, Volcanism, and Changes in Atmospheric CO2, The Carbon Cycle and Atmospheric CO2: Natural Variations Archean to Present, pp. 504-529.

Arthur, M.A., Dean, W.E., Pratt, L.M., 1988. Geochemical and climatic effects of increased marine organic carbon burial at the Cenomanian/Turonian boundary. Nature 335, 714.

Arthur, M.A., Sageman, B.B., 1994. Marine Black Shales: Depositional Mechanisms and Environments of Ancient Deposits. Annu. Rev. Earth Planet. Sci. 22, 499-551.

Bata, T., 2016. Evidences of widespread cretaceous deep weathering and its consequences: a review. Earth Science Research 5, 69-84.

Beil, S., Kuhnt, W., Holbourn, A.E., Aquit, M., Flögel, S., Chellai, E.H., Jabour, H., 2018. New insights into Cenomanian paleoceanography and climate evolution from the Tarfaya Basin, southern Morocco. Cretaceous Research 84, 451-473.

Berner, R.A., 2006. GEOCARBSULF: A combined model for Phanerozoic atmospheric O2 and CO2. Geochimica et Cosmochimica Acta 70, 5653-5664.

Bjerrum, C.J., Bendtsen, J., Legarth, J.J.F., 2006. Modeling organic carbon burial during sea level rise with reference to the Cretaceous. Geochemistry, Geophysics, Geosystems 7.

Blume, H.-P., 1988. The fate of iron during soil formation in humid-temperate environments, Iron in soils and clay minerals. Springer, pp. 749-777.

Brandes, J.A., Devol, A.H., 2002. A global marine-fixed nitrogen isotopic budget: Implications for Holocene nitrogen cycling. Global Biogeochemical Cycles 16, 67-61-67-14.

Brüchert, V., Jørgensen, B.B., Neumann, K., Riechmann, D., Schlösser, M., Schulz, H., 2003. Regulation of bacterial sulfate reduction and hydrogen sulfide fluxes in the central namibian coastal upwelling zone. Geochimica et Cosmochimica Acta 67, 4505-4518.

Brumsack, H.J., 2006. The trace metal content of recent organic carbon-rich sediments: Implications for Cretaceous black shale formation. Palaeogeography, Palaeoclimatology, Palaeoecology 232, 344-361.

Canfield, D.E., Raiswell, R., Westrich, J.T., Reaves, C.M., Berner, R.A., 1986. The use of chromium reduction in the analysis of reduced inorganic sulfur in sediments and shales. Chemical Geology 54, 149-155.

Clarkson, M.O., Stirling, C.H., Jenkyns, H.C., Dickson, A.J., Porcelli, D., Moy, C.M., Pogge von Strandmann, P.A.E., Cooke, I.R., Lenton, T.M., 2018. Uranium isotope evidence for two episodes of deoxygenation during Oceanic Anoxic Event 2. Proceedings of the National Academy of Sciences.

Clarkson, M.O., Wood, R.A., Poulton, S.W., Richoz, S., Newton, R.J., Kasemann, S.A., Bowyer, F., Krystyn, L., 2016. Dynamic anoxic ferruginous conditions during the end-Permian mass extinction and recovery. Nat Commun 7.

Craggs, H.J., Valdes, P.J., Widdowson, M., 2012. Climate model predictions for the latest Cretaceous: An evaluation using climatically sensitive sediments as proxy indicators. Palaeogeography, Palaeoclimatology, Palaeoecology 315-316, 12-23.

Dale, A.W., Sommer, S., Lomnitz, U., Montes, I., Treude, T., Liebetrau, V., Gier, J., Hensen, C., Dengler, M., Stolpovsky, K., 2015. Organic carbon production, mineralization and preservation on the Peruvian margin. Biogeosciences (BG) 12, 1537-1559.

Diaz, R.J., Rosenberg, R., 2008. Spreading Dead Zones and Consequences for Marine Ecosystems. Science 321, 926-929.

Dickson, A.J., Jenkyns, H.C., Porcelli, D., van den Boorn, S., Idiz, E., 2016. Basin-scale controls on the molybdenum-isotope composition of seawater during Oceanic Anoxic Event 2 (Late Cretaceous). Geochimica et Cosmochimica Acta 178, 291-306.

Dickson, A.J., Rees-Owen, R.L., März, C., Coe, A.L., Cohen, A.S., Pancost, R.D., Taylor, K., Shcherbinina, E., 2014. The spread of marine anoxia on the northern Tethys margin during the Paleocene-Eocene Thermal Maximum. Paleoceanography 29, 2014PA002629.

Einsele, G., Wiedmann, J., 1982. Turonian black shales in the Moroccan coastal basins: first upwelling in the Atlantic Ocean?, Geology of the northwest African continental margin. Springer, pp. 396-414.

Flögel, S., Wallmann, K., Poulsen, C.J., Zhou, J., Oschlies, A., Voigt, S., Kuhnt, W., 2011. Simulating the biogeochemical effects of volcanic CO_2 degassing on the oxygen-state of the deep ocean during the Cenomanian/Turonian Anoxic Event (OAE2). Earth and Planetary Science Letters 305, 371-384.

Fossing, H., Gallardo, V.A., Jørgensen, B.B., Hüttel, M., Nielsen, L.P., Schulz, H., Canfield, D.E., Forster, S., Glud, R.N., Gundersen, J.K., Küver, J., Ramsing, N.B., Teske, A., Thamdrup, B., Ulloa, O., 1995. Concentration and transport of nitrate by the mat-forming sulphur bacterium Thioploca. Nature 374, 713.

Gruber, N., Sarmiento, J.L., 1997. Global patterns of marine nitrogen fixation and denitrification. Global Biogeochemical Cycles 11, 235-266.

Hay, W.W., 2008. Evolving ideas about the Cretaceous climate and ocean circulation. Cretaceous Research 29, 725-753.

Hay, W.W., DeConto, R.M., de Boer, P., Flögel, S., Song, Y., Stepashko, A., 2019. Possible solutions to several enigmas of Cretaceous climate. International Journal of Earth Sciences, in press.

Higgins, M.B., Robinson, R.S., Husson, J.M., Carter, S.J., Pearson, A., 2012. Dominant eukaryotic export production during ocean anoxic events reflects the importance of recycled NH4+. Proceedings of the National Academy of Sciences 109, 2269-2274.

Jenkyns, H.C., 2010. Geochemistry of oceanic anoxic events. Geochemistry Geophysics Geosystems 11, Q03004, doi:03010.01029/02009GC002788.

Jenkyns, H.C., Dickson, A.J., Ruhl, M., Boorn, S.H.J.M., 2017. Basalt-seawater interaction, the Plenus Cold Event, enhanced weathering and geochemical change: deconstructing Oceanic Anoxic Event 2 (Cenomanian-Turonian, Late Cretaceous). Sedimentology 64, 16-43.

Junium, C.K., Arthur, M.A., 2007. Nitrogen cycling during the Cretaceous, Cenomanian-Turonian Oceanic Anoxic Event II. Geochemistry Geophysics Geosystems 8, Q03002, doi:10.1029/2006GC001328.

Keeling, R.F., Körtzinger, A., Gruber, N., 2011. Ocean Deoxygenation in a Warming World. Annual Review of Marine Science 2, 199-229.

Knoll, A.H., Bambach, R.K., Canfield, D.E., Grotzinger, J.P., 1996. Comparative Earth History and Late Permian Mass Extinction. Science 273, 452-457.

Kolonic, S., Wagner, T., Forster, A., Sinninghe Damsté, Walsworth-Bell, B., Erba, E., Turgeon, S., Brumsack, H.-J., Chellai, E.H., Tsikos, H., Kuhnt, W., Kuypers, M.M.M., 2005. Black shale deposition on the northwest African Shelf during the Cenomanian/Turonian oceanic anoxic event: Climate coupling and global organic carbon burial. Paleoceanography 20.

Kuhnt, W., Nederbragt, A., Leine, L., 1997. Cyclicity of Cenomanian-Turonian organic-carbon-rich sediments in the Tarfaya Atlantic Coastal Basin (Morocco). Cretaceous Research 18, 587-601.

Kuhnt, W., Chellai, E.H., Holbourn, A., Luderer, F., Thurow, J., Wagner, T., El Albani, A., Beckmann, B., Herbin, J.-P., Kawamura, H., Kolonic, S., Nederbragt, S., Street, C., Ravilious, K., 2001. Morocco Basin's sedimentary record may provide correlations for Cretaceous paleoceanographic events worldwide. Eos, Transactions American Geophysical Union 82, 361-364.

Kuhnt, W., Holbourn, A.E., Beil, S., Aquit, M., Krawczyk, T., Flögel, S., Chellai, E.H., Jabour, H., 2017. Unraveling the onset of Cretaceous Oceanic Anoxic Event 2 in an extended sediment archive from the Tarfaya-Laayoune Basin, Morocco. Paleoceanography 32, 923-946.

Kuypers, M.M.M., Pancost, R.D., Damsté, J.S.S., 1999. A large and abrupt fall in atmospheric CO_2 concentration during Cretaceous times. Nature 399, 342.

Lehmann, M.F., Sigman, D.M., Berelson, W.M., 2004. Coupling the $^{15}N/^{14}N$ and $^{18}O/^{16}O$ of nitrate as a constraint on benthic nitrogen cycling. Marine Chemistry 88, 1-20.

Lyons, T.W., Severmann, S., 2006. A critical look at iron paleoredox proxies: New insights from modern euxinic marine basins. Geochimica et Cosmochimica Acta 70, 5698-5722.

595 März, C., Poulton, S.W., Beckmann, B., Küster, K., Wagner, T., Kasten, S., 2008. Redox sensitivity of P cycling during marine black shale formation: Dynamics of sulfidic and anoxic, non-sulfidic bottom waters. Geochimica et Cosmochimica Acta 72, 3703-3717.

McLennan, S.M., 2001. Relationships between the trace element composition of sedimentary rocks and upper continental crust. Geochemistry Geophysics Geosystems 2.

600 Meyer, K.M., Kump, L.R., 2008. Oceanic euxinia in Earth history: Causes and consequences. Annu. Rev. Earth Planet. Sci. 36, 251-288.

Mollier-Vogel, E., Ryabenko, E., Martinez, P., Wallace, D., Altabet, M.A., Schneider, R., 2012. Nitrogen isotope gradients off Peru and Ecuador related to upwelling, productivity, nutrient uptake and oxygen deficiency. Deep Sea Research Part I: Oceanographic Research Papers 70, 14-25.

605 Monteiro, F.M., Pancost, R.D., Ridgwell, A., Donnadieu, Y., 2012. Nutrients as the dominant control on the spread of anoxia and euxinia across the Cenomanian-Turonian oceanic anoxic event (OAE2): Model-data comparison. Paleoceanography 27.

Mort, H.P., Adatte, T., Keller, G., Bartels, D., Föllmi, K.B., Steinmann, P., Berner, Z., Chellai, E.H., 2008. Organic carbon deposition and phosphorus accumulation during Oceanic Anoxic Event 2 in
610 Tarfaya, Morocco. Cretaceous Research 29, 1008-1023.

Müller, R.D., Sdrolias, M., Gaina, C., Roest, W.R., 2008. Age, spreading rates, and spreading asymmetry of the world's ocean crust. Geochemistry Geophysics Geosystems 9, Q04006, doi:04010.01029/02007GC001743.

Oschlies, A., Brandt, P., Stramma, L., Schmidtko, S., 2018. Drivers and mechanisms of ocean
615 deoxygenation. Nature Geoscience 11, 467–473.

Ostrander, C.M., Owens, J.D. and Nielsen, S.G. (2017) Constraining the rate of oceanic deoxygenation leading up to a Cretaceous Oceanic Anoxic Event (OAE-2: ~94 Ma). Science Advances 3, 10.1126/sciadv.1701020.

Owens, J.D., Reinhard, C.T., Rohrssen, M., Love, G.D., Lyons, T.W., 2016. Empirical links between trace metal cycling and marine microbial ecology during a large perturbation to Earth's carbon cycle. Earth and Planetary Science Letters 449, 407-417.

Pogge von Strandmann, P.A.E., Jenkyns, H.C., Woodfine, R.G., 2013. Lithium isotope evidence for enhanced weathering during Oceanic Anoxic Event 2. Nature Geoscience 6, 668–672.

Poulton, S.W., Canfield, D.E., 2011. Ferruginous conditions: A dominant feature of the ocean through Earth's history. ELEMENTS 7, 107-112.

Poulton, S.W., Canfield, D.E., 2005. Development of a sequential extraction procedure for iron: implications for iron partitioning in continentally derived particulates. Chemical Geology 214, 209-221.

Poulton, S.W., Henkel, S., März, C., Urquhart, H., Flögel, S., Kasten, S., Sinninghe Damsté, J.S., Wagner, T., 2015. A continental-weathering control on orbitally driven redox-nutrient cycling during Cretaceous Oceanic Anoxic Event 2. Geology 43, 963-966.

Raiswell, R., Canfield, D.E., 1996. Rates of reaction between silicate iron and dissolved sulfide in Peru Margin sediments. Geochimica et Cosmochimica Acta 60, 2777-2787.

Raiswell, R., Canfield, D.E., 1998. Sources of iron for pyrite formation in marine sediments. American Journal of Science 298, 219-245.

Ronov, A.B., 1994. Phanerozoic transgressions and regressions on the continents; a quantitative approach based on areas flooded by the sea and areas of marine and continental deposition. American Journal of Science 294, 777-801.

Royer, D.L., Donnadieu, Y., Park, J., Kowalczyk, J., GoddÃ©ris, Y., 2014. Error analysis of CO2 and O2 estimates from the long-term geochemical model GEOCARBSULF. American Journal of Science 314, 1259-1283.

Schmidtko, S., Stramma, L., Visbeck, M., 2017. Decline in global oceanic oxygen content during the past five decades. Nature 542, 335-339.

Scholz, F., 2018. Identifying oxygen minimum zone-type biogeochemical cycling in Earth history using inorganic geochemical proxies. Earth-Science Reviews 184, 29-45.

Scholz, F., Löscher, C.R., Fiskal, A., Sommer, S., Hensen, C., Lomnitz, U., Wuttig, K., Göttlicher, J., Kossel, E., Steininger, R., Canfield, D.E., 2016. Nitrate-dependent iron oxidation limits iron transport in anoxic ocean regions. Earth and Planetary Science Letters 454, 272-281.

Scholz, F., Severmann, S., McManus, J., Noffke, A., Lomnitz, U., Hensen, C., 2014. On the isotope composition of reactive iron in marine sediments: Redox shuttle versus early diagenesis. Chemical Geology 389, 48-59.

Schulz, H.N., Brinkhoff, T., Ferdelman, T.G., MarinÃ©, M.H.n., Teske, A., JÃ¸rgensen, B.B., 1999. Dense Populations of a Giant Sulfur Bacterium in Namibian Shelf Sediments. Science 284, 493-495.

Schunck, H., Lavik, G., Desai, D.K., Grosskopf, T., Kalvelage, T., Loescher, C.R., Paulmier, A., Contreras, S., Siegel, H., Holtappels, M., Rosenstiel, P., Schilhabel, M.B., Graco, M., Schmitz, R.A., Kuypers, M.M.M., LaRoche, J., 2013. Giant hydrogen sulfide plume in the oxygen minimum zone off Peru supports chemolithoautotrophy. Plos One 8, e68661. doi:10.1371/journal.pone.0068661.

Schwertmann, U., 1988. Occurrence and formation of iron oxides in various pedoenvironments, Iron in soils and clay minerals. Springer, pp. 267-308.

Sigman, D.M., Robinson, R., Knapp, A.N., van Geen, A., McCorkle, D.C., Brandes, J.A., Thunell, R.C., 2003. Distinguishing between water column and sedimentary denitrification in the Santa Barbara Basin using the stable isotopes of nitrate. Geochemistry, Geophysics, Geosystems 4.

Sinninghe Damsté, J.S. and Köster, J. (1998) A euxinic southern North Atlantic Ocean during the Cenomanian/Turonian oceanic anoxic event. Earth and Planetary Science Letters 158, 165-173.

Trabucho Alexandre, J., Tuenter, E., Henstra, G.A., van der Zwan, K.J., van de Wal, R.S.W., Dijkstra, H.A., de Boer, P.L., 2010. The mid-Cretaceous North Atlantic nutrient trap: Black shales and OAEs. Paleoceanography 25, PA4201, doi:4210.1029/2010PA001925.

Wallmann, K., 2001. Controls on the cretaceous and cenozoic evolution of seawater composition, atmospheric CO2 and climate. Geochimica et Cosmochimica Acta 65, 3005-3025.

Wang, Y., Huang, C., Sun, B., Quan, C., Wu, J., Lin, Z., 2014. Paleo-CO_2 variation trends and the Cretaceous greenhouse climate. Earth-Science Reviews 129, 136-147.

Westermann, S., Vance, D., Cameron, V., Archer, C., Robinson, S.A., 2014. Heterogeneous oxygenation states in the Atlantic and Tethys oceans during Oceanic Anoxic Event 2. Earth and Planetary Science Letters 404, 178-189.

Widdowson, M., 2007. Laterite and Ferricrete, in: David, J.N., Sue, J.M. (Eds.), Geochemical Sediments and Landscapes.

Figure captions

Figure 1. Bathymetric maps showing the location of the Tarfaya Basin and DSDP Site 367 within (A) the Proto-North Atlantic during the Cenomanian-Turonian interval (reconstructed after Müller et al. (2008)) and (B) the present-day North Atlantic Ocean (bathymetric data from GEBCO). The locations of drill cores SN4, S13, S57, S75 and the outcrop Mohammed Plage are depicted in a close-up map in (C).

Figure 2. (A) Geochemical proxy records of core SN4 from the Tarfaya Basin: Isotope composition of organic carbon ($\delta^{13}C_{org}$) (data from Beil et al., 2018), TOC, bulk $\delta^{15}N$, Fe_{HR}/Fe_T (vertical dashed line represents threshold for anoxic conditions), Fe_{py}/Fe_{HR} (vertical dashed line represents threshold for euxinic conditions), Fe_T/Al (vertical dashed line represents UCC), V_{XS}, Mo_{XS} and $log(V/Mo)_{XS}$. Trace metal concentration ratios are given as logarithmic ratios to avoid asymmetry effects. The horizontal

gray array depicts the duration of OAE2, as defined by the $\delta^{13}C_{org}$ excursion (76 - 110 m). The horizontal line within this array depicts the timing of the Plenus Cold Event (PCE) (after Kuhnt et al. (2017)). See Beil et al. (2018) for further stratigraphic information. (B) Close-up of geochemical proxy records of core SN4 from the Tarfaya Basin highlighting the time period immediately before and during OAE2. The data shown in this figure are contained in the Electronic Annex.

Figure 3. Lateral distribution of Fe_{HR}/Fe_T and Fe_{py}/Fe_{HR} at the southeastern margin of the Proto-North Atlantic before/after and during OAE2. The gray bars depict the threshold range for anoxic (Fe_{HR}/Fe_T > 0.22 - 0.38) and euxinic (Fe_{HR}/Fe_T > 0.7 - 0.8) conditions in the water column (Poulton and Canfield, 2011). A combination of Fe_{HR}/Fe_T > 0.38 and Fe_{HR}/Fe_T < 0.7 is considered indicative of ferruginous conditions. Data for DSDP Site 367 and S57 are from Westermann et al. (2014) and Poulton et al. (2015). The Fe_{py}/Fe_{HR} data for DSDP Site 367 were corrected for pyrite oxidation during sample storage (see Westermann et al. (2014) for details). The Fe_{HR}/Fe_T and Fe_{py}/Fe_{HR} of sediments from the Peruvian margin are shown for comparison (data from Scholz et al. (2014)).

Figure 4. Plots of Fe_T/Al versus Fe_{HR}/Fe_T featuring two different models of how elevated concentrations of sedimentary reactive Fe in the Cretaceous Proto-North Atlantic were generated: (A) Deposition of reactive Fe minerals that are precipitated in the water column. The scenarios were calculated using Equations (1) and (2) adopting MAR = 0.01 g cm yr^{-1}, Al = 30 mg g^{-1}, RR_{Fe} = 0.00 - 0.011 mmol cm^{-2} yr^{-1} and variable $(Fe_T/Al)_{in}$ and $(Fe_{HR}/Fe_T)_{in}$ as initial values. Generating the observed range of reactive Fe enrichments with this scenario requires a broad range of initial values (i.e., terrigenous input), mostly above the threshold value for anoxic and euxinic or ferruginous conditions (Poulton and Canfield, 2011). (B) Mixing array between UCC (McLennan, 2001), modern continental margin sediments with oxic bottom water (Raiswell and Canfield, 1998) and data for two laterite profiles in India (Widdowson, 2007). The mixing array was calculated using Equations (3) and (4). The range of Fe_{HR}/Fe_T of laterite samples was approximated based on mineralogical data and ternary diagrams of SiO_2, Al_2O_3 and Fe_2O_3. The broad range of Fe_T/Al reflects differences in precursor rocks (basalt versus greywacke) and the transition from a kaolinite- to Fe (oxyhydr)oxide-dominated

715 weathering assemblage towards the top of the profiles (Widdowson, 2007). Iron speciation data for DSDP Site 367 and S57 are from Westermann et al. (2014) and Poulton et al. (2015).

Figure 5. Evolution of Fe_{HR}/Fe_T as a function of the authigenic Fe rain rate. The two scenarios were calculated based on Equation (2) using the Al concentration and MAR of the Tarfaya upwelling system during OAE2 and the Peru margin (Table 1). Initial values correspond to the average Fe_T/Al 720 and Fe_{HR}/Fe_T below a stratigraphic depth of 230 m (Tarfaya) and UCC/modern continental margin sediment with oxic bottom water (Peru). Circles depict the average Fe_{HR}/Fe_T in Tarfaya above 230 m downcore depth and Peru margin sediments at 145 m (Scholz et al, 2014).

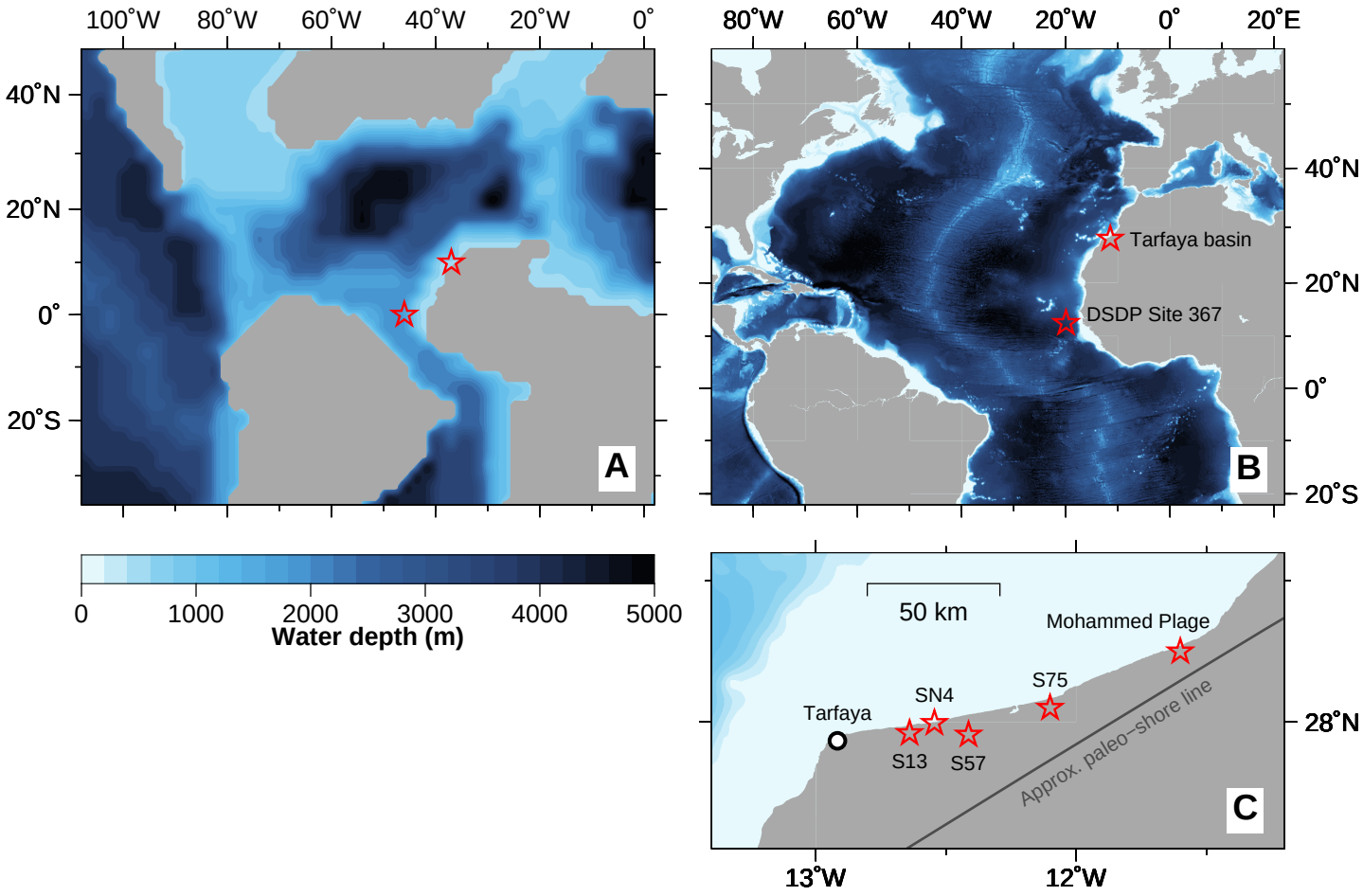
100°W
80°W
60°W
40°W
20°W
0°
40°N
20°N
0°
20°S
A
0
1000
2000
3000
4000
5000
Water depth (m)
80°W
60°W
40°W
20°W
0°
20°E
40°N
20°N
0°
20°S
Tarfaya basin
DSDP Site 367
B
50 km
Mohammed Plage
S75
SN4
Tarfaya
S13
S57
Approx. paleo−shore line
C
28°N
13°W
12°W

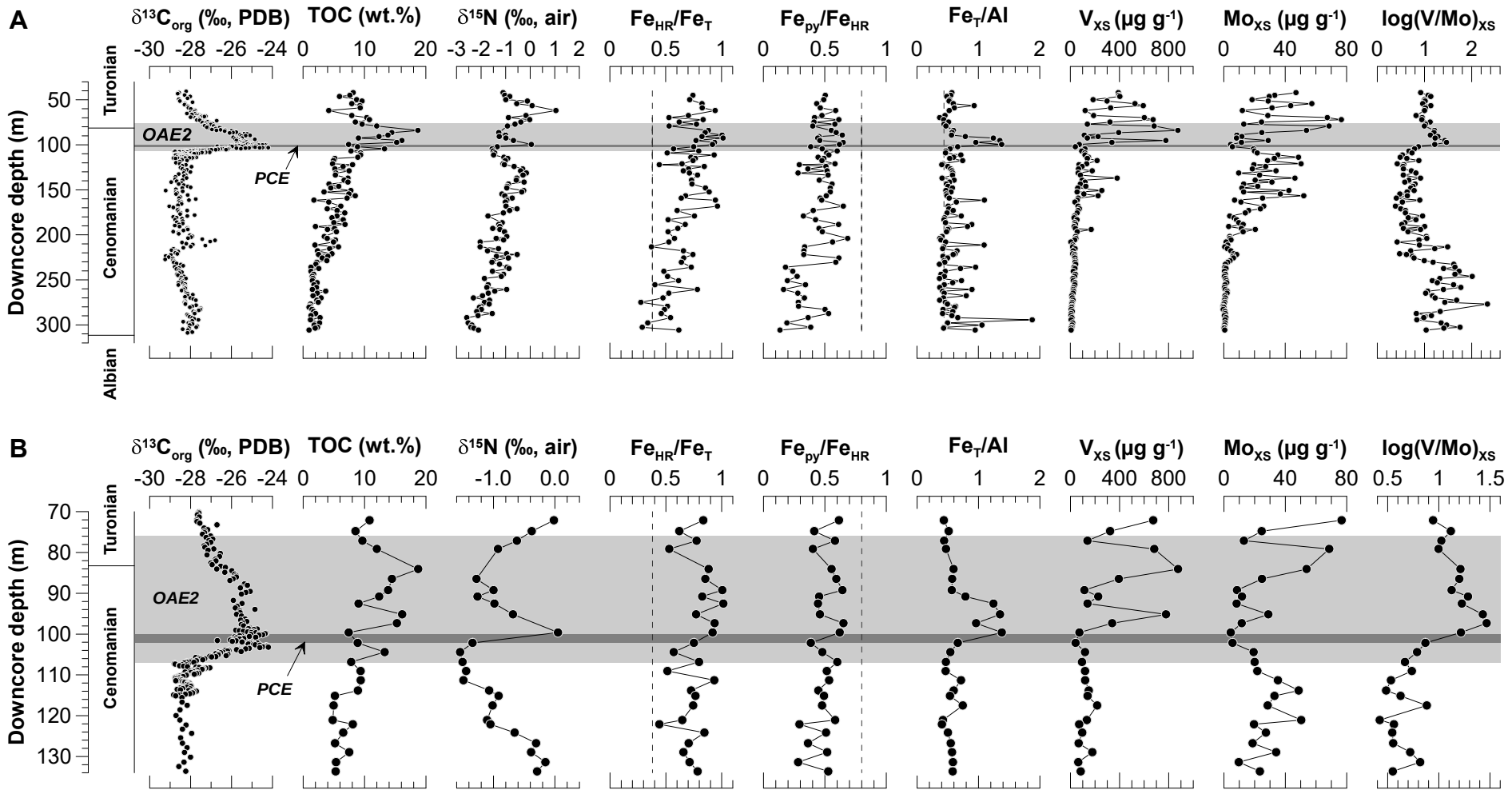
A
δ13Corg (‰, PDB)
TOC (wt.%)
δ15N (‰, air)
FeHR/FeT
FePy/FeHR
FeT/Al
VXS (µg g-1)
MoXS (µg g-1)
log(V/Mo)XS
Downcore depth (m)
Turonian
Cenomanian
Albian
OAE2
PCE
B
δ13Corg (‰, PDB)
TOC (wt.%)
δ15N (‰, air)
FeHR/FeT
FePy/FeHR
FeT/Al
VXS (µg g-1)
MoXS (µg g-1)
log(V/Mo)XS
Downcore depth (m)
Turonian
Cenomanian
OAE2
PCE

Figure 2

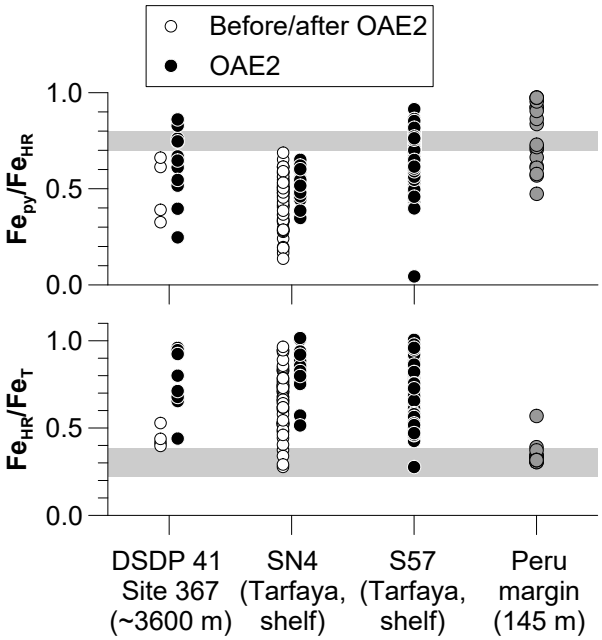
Before/after OAE2
OAE2
1.0
0.5
0.0
Fe_{py}/Fe_{HR}
1.0
0.5
0.0
Fe_{HR}/Fe_T
DSDP 41 Site 367 (~3600 m)
SN4 (Tarfaya, shelf)
S57 (Tarfaya, shelf)
Peru margin (145 m)

Figure 3

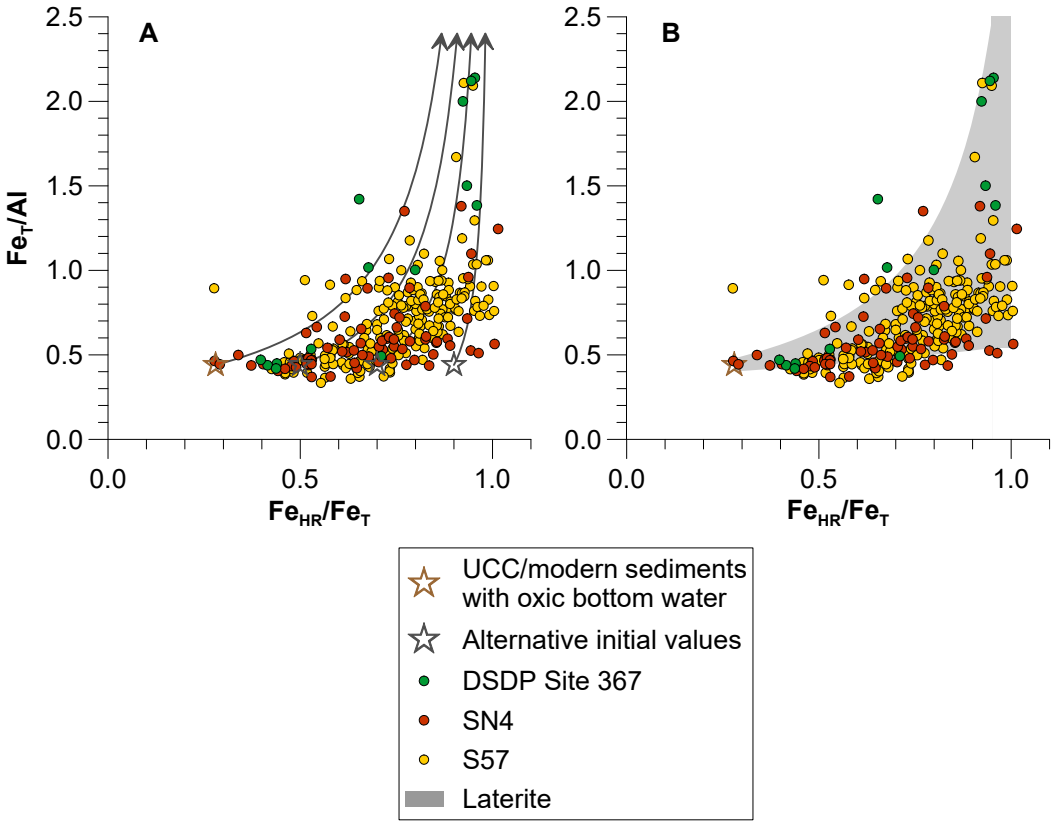
A
B
2.5
2.0
1.5
1.0
0.5
0.0
0.0
0.5
1.0
Fe_T/Al
Fe_HR/Fe_T
UCC/modern sediments with oxic bottom water
Alternative initial values
DSDP Site 367
SN4
S57
Laterite

Figure 4

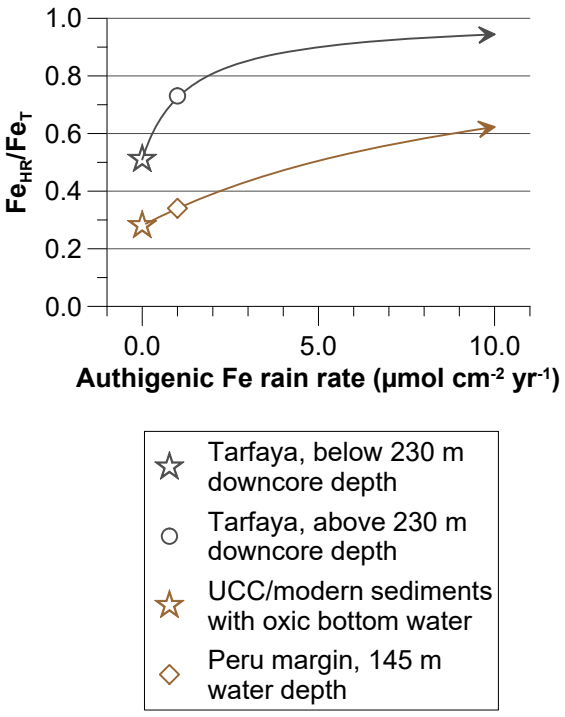
1.0
0.8
0.6
0.4
0.2
0.0
Fe_{HR}/Fe_T
0.0
5.0
10.0
Authigenic Fe rain rate (µmol cm^{-2} yr^{-1})
Tarfaya, below 230 m downcore depth
Tarfaya, above 230 m downcore depth
UCC/modern sediments with oxic bottom water
Peru margin, 145 m water depth

Figure 5

Table 1. Sedimentary TOC, Fe_T, Al and Fe_{HR} and the corresponding mass accumulation rates in the Cenomanian-Turonian Proto-North Atlantic and on the Peru margin during the late Holocene.

	MAR	TOC	SD	Fe_T	SD	Al	SD	n	Fe_{HR}	SD	n	TOC-MAR[5]	SD	Fe_T-MAR	SD	Al-MAR	SD	Fe_{HR}-MAR	SD
	($g\ cm^{-2}\ kyr^{-1}$)	(wt.%)		($mg\ g^{-1}$)		($mg\ g^{-1}$)			(mg g-1)			($g\ cm^{-2}\ kyr^{-1}$)		($mg\ cm^{-2}\ kyr^{-1}$)		($mg\ cm^{-2}\ kyr^{-1}$)		($mg\ cm^{-2}\ kyr^{-1}$)	
SN4[1], OAE2	15.4	11.4	3.1	6.9	8.4	8.2	6.1	12	5.3	7.2	15	1.76	0.48	106	129	127	94	81	110
SN4, pre-OAE2	9.0	3.9	2.2	18.3	10.3	33.4	19.0	83	10.5	5.8	49	0.35	0.19	165	93	301	171	95	52
S57[2], OAE2	6.0	8.5	4.6	6.4	13.0	7.9	6.1	207	4.4	6.5	207	0.51	0.27	38	78	47	37	26	39
DSDP Site 367[3], OAE2	4.0	25.7	10.8	28.1	7.1	26.1	12.3	10	24.1	9.0	10	1.03	0.43	113	29	104	49	96	36
DSDP Site 367, pre-OAE2	4.0	9.3	4.3	29.0	7.6	63.3	19.1	4	12.7	2.7	4	0.37	0.17	116	30	253	76	51	11
Peru margin[4] 145 m, late Holocene	28.0	7.3	1.3	22.0	3.2	49.9	7.2	18	7.4	1.1	18	2.05	0.37	617	91	1400	200	200	30

[1]MAR from Kuhnt et al. (2017).

[2]MAR from Kolonic et al. (2005); geochemical data from Poulton et al. (2015).

[3]Approximate MAR from Lancelot et al. (1978); geochemical data from Westermann et al. (2014).

[4]MAR from Scholz et al. (2011); geochemical data from Scholz et al., (2014).

[5]Element MARs were calculated by multiplying MAR with element concentration.